Bistatic Radar Scattering From an Ocean Surface at L-band

Ahmad AWADA, Ali KHENCHAF and Arnaud COATANHAY
ENSIETA (Ecole Nationale Superieure des Ingenieurs des Etudes et Techniques d'Armement)
Laboratory E^3I^2 EA-3876, 2 rue Francois Verny 29806 Brest Cedex 09 France
Email: {awadaah, ali.khenchaf, arnaud.coatanhay}@ensieta.fr

***Abstract*— This paper presents a numerical analysis for bistatic scattering from the sea surface at L-band. The unifying scattering model Small Slope Approximation (SSA) of the first order is applied to calculate normalized bistatic cross section (NBCS) of the ocean surface. The calculations were made by assuming the surface-height spectrum of Elfouhaily *et al*. The correlation function based on this spectrum is calculated. The negative region participation in surface scattering which is function of the incident angle, the wind speed and the exploring wavelength is discussed. A comparison between SSA and geometric optics models shows that the last one is generally not accurate at L-band especially at large angles of incidences. Numerical results examine the wind dependency over a wide range of incident angles along the specular direction and in the forward scattering configuration. In addition, the NBCS behavior in fully bistatic configuration is predicted. Numerical results are obtained as a function of wind speed, incident/scattering angles and polarization states.**

I. INTRODUCTION

Usually remote sensing applications are based on radar systems operating in C, X- and K_u-bands. Recently, the L-band signal frequency received in interest importance in these application in view of the availability of the Global System Positioning (GPS). Though, the GPS signals reflected from the ocean surface have potential use for various remote sensing purposes. Some possibilities are measurements of surface roughness characteristics from which wave height, wind speed, and direction could be determined [1][2]. The concept proposes that a similar technique to that of traditional radar remote sensing can be applied to bistatically reflected signals transmitted from global navigation satellites, such as those of the GPS system and in the future those of the Galileo navigation constellation.

Basically, the received power can be represented by an appropriate form of the radar equation containing the bistatic scattering coefficient at L-band. Hence, any attempt to recover sea state parameters requires understanding the scattering process for general sea state conditions and direction of incidence.

In ocean remote sensing applications (wind retrieval, weather forecasting, $\cdots$), the basic idea of the technique relies on the assumption that the ocean surface normalized radar cross section is strongly correlated with the local surface wind speed and direction [3]. These applications require the development of accurate models to predict the radar scattering from such surfaces. Zavorotny *et al* treat this problem using the geometric optics limit of the Kirchhoff Approximation (KA-GO), Fung *et al* applied the Integral Equation Model (IEM) [4], where Coatanhay *et al* applied the Two Scale Model (TSM) in this context [5]. Recently there is an improved geometrical optics model suggested by Thompson *et al* [6]. So, in this study we treat this problem with the SSA model. It is an unifying theory that could reconcile Small Perturbation method (SPM) and Kirchhoff Approximation (KA). The SSA can be applied to an arbitrary wavelength, provided the tangent of grazing angles of incident/scattered radiation sufficiently exceeds RMS slopes of roughness.

In section II, we discussed the scattering dependence on the key parameters (wave components, $\cdots$). In section III, we analyze the sea correlation function based on the Elfouhaily model for the sea roughness spectrum. The contribution of the negative portion on the NBCS is discussed. Finally, we present numerical results in several configurations: along the specular direction, in the forward case and in the fully bistatic case in both co- and cross-polarization.

II. SCATTERING DEPENDENCE ON KEY PARAMETERS

Many approaches were developed to evaluate the electromagnetic scattering from a rough surface, each is available in certain hypothesis and conditions. It must be noted that the approximate models are still a necessity due to the insurmountable numerical complexity of realistic scattering problems. We can refer to [7] which is the latest critical and up-to-date survey of the analytical approximate. Geometrical configuration adopted to resolve the wave-scattering problem from the sea surface is given in figure 1.

So, in this paper we choose the SSA model to treat the scattering problem from the sea surface. It is an appropriate model for scattering from large-(Kirchoff regime), intermediate- and small-scale (the Bragg regime) roughness within a single theoretical scheme. The SSA can be applied for an arbitrary wavelength, provided the tangent of grazing angles of incident/scattered radiation sufficiently exceeds the rms (root mean square) slopes of roughness. It is noteworthy that slopes of sea-surface roughness are generally small except for steep breaking waves [8]. Another advantage of the SSA is that it represents regular expansion with respect to powers of slopes. SSA model does not introduce a scale-dividing parameter k_d separating small- and large-scale components of the roughness as it is the case in the Two Scale Model (TSM)

0-7803-9497-6/06/$20.00 © 2006 IEEE.

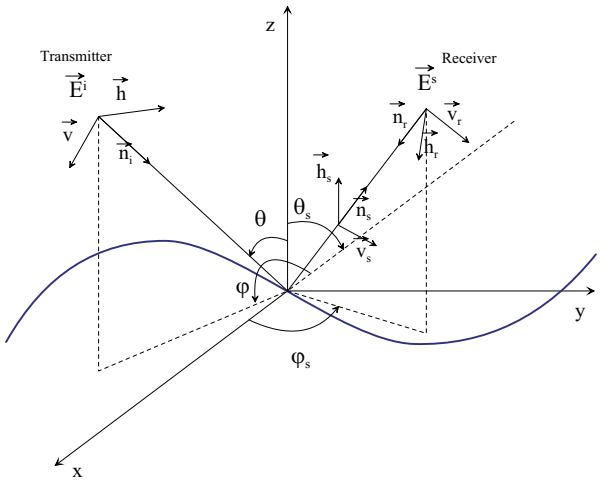

Fig. 1. Geometrical con guration for the wave-scattering from sea surface

[9]. In the backscattering con guration this parameter can be chosen within wide limits [8] which range from $k/1.5$ to $k/40$; where $k = 2\pi/\lambda$ is the electromagnetic wavenumber. In this context, the single theoretical scheme of the SSA make it a credible model especially in bistatic con guration [10].

We show in this section that a radar system operating in the microwave bands may be sensitive only to a portion of the surface correlation (coherent contribution). For this reason, the effective surface parameters exist consequently. The particular portion of the correlation sensed is determined by the exploring wavelength, the incident angle, the state of the sea, and the decay rate of the correlation function itself. To point out this dependence consider the bistatic incoherent scattering coef cient under the small slope approximation (SSA) at the rst order [8] :

$$\sigma_{\alpha\alpha_0}(\boldsymbol{k},\boldsymbol{k}_0) = \frac{1}{\pi}\left|\frac{2q_k\ q_0}{q_k+q_0}B_{\alpha\alpha_0}(\boldsymbol{k},\boldsymbol{k}_0)\right|^2 \cdot e^{-(q_k+q_0)^2\rho(0)} \times \int \left\{\exp[(q_k+q_0)^2\rho(\boldsymbol{r})]-1\right\}\exp[-i(\boldsymbol{k}-\boldsymbol{k}_0)\boldsymbol{r}]\mathrm{d}\boldsymbol{r} \quad (1)$$

where $\boldsymbol{k}_0, q_0$ are horizontal and vertical projections of the wave vector of an incident wave, and $\boldsymbol{k}, q$ are appropriate components of the wave vector of scattered wave. $B_{\alpha\alpha_0}(\boldsymbol{k},\boldsymbol{k}_0)$ is a non-singular dimensionless function depending on polarization. Explicit expressions for it can be found in [11]. α, α_0 corresponds to the polarization of scattered and incident plane wave respectively. Nevertheless, $\rho(\boldsymbol{r})$ is the correlation function of the rough surface $z(\boldsymbol{r})$. For an isotropically rough surface, (1) can be simpli ed as follows:

$$\sigma_{\alpha\alpha_0}(\boldsymbol{k},\boldsymbol{k}_0) = 2\left|\frac{2q_k\ q_0}{q_k+q_0}B_{\alpha\alpha_0}(\boldsymbol{k},\boldsymbol{k}_0)\right|^2 \cdot e^{-(q_k+q_0)^2\rho(0)} \times \int_0^{2\pi}\frac{d\phi}{2\pi}\int_0^{\infty}\left\{\exp[(q_k+q_0)^2\rho(r)]-1\right\} \times \exp[-i(k_x-k_{0x})\cos\phi - i(k_y-k_{0y})\sin\phi]\ r\ \mathrm{d}r \quad (2)$$

Where

θ, φ and θ_s, φ_s	incident and scattering directions, respectively
k	electromagnetic wavenumber and

$$\begin{aligned} q_k \equiv q = k\cos\theta \quad &, \quad q_0 = k\cos\theta \\ k_x = k\sin\theta_s\cos\varphi_s \ &, \quad k_{0x} = k\sin\theta\cos\varphi \\ k_y = k\sin\theta_s\sin\varphi_s \ &, \quad k_{0y} = k\sin\theta\sin\varphi \end{aligned}$$

The phase factor in (2) has the form

$$\exp[-jKr\cos\varphi\cos\phi - jKr\sin\varphi\sin\phi] = exp[-iKr\cos(\varphi-\phi)]$$

where

$$K = \sqrt{(k_x-k_{0x})^2+(k_y-k_{0y})^2}$$

As the coef cient of diffusion must be a real value one takes only the real part of the previous phase, thus by using the real part of the Bessel generating function de ned in [12], we have

$$\sigma_{\alpha\alpha_0}(\boldsymbol{k},\boldsymbol{k}_0) = 2\left|\frac{2q_k\ q_0}{q_k+q_0}B_{\alpha\alpha_0}(\boldsymbol{k},\boldsymbol{k}_0)\right|^2 \cdot \int_0^{\infty}\{e^{-\kappa[\rho(0)-\rho(r)]}-e^{-\kappa\rho(0)}\}J_0(Kr)r\mathrm{d}r \quad (3)$$

where $\kappa = (q_k+q_0)^2$.

To highlight the importance of the range of r in the integration on $\sigma_{\alpha\alpha_0}$ in specular direction case ($\theta=\theta_s, \varphi=\varphi_s$), we plot the integrand in the curly bracket in (3) versus r in gure 2 at an incident angle $\theta = 60°$, where we used a correlation function calculated from Elfouhaily's spectrum [13]. The case (a) shows that the value of r over which the integrand is signi cant is about 2 m for L-band signals (F=1.58 GHz). Under this condition, only points on the surface less than 2 m apart remain correlated in their scattering contribution. For signals in K_u-band (F=14 GHz), the signi cant integration range of r is reduced to about 0.15 m. In the case (b) we point out the wind dependence on the integration range of r in L-band at normal incidence. It is clear that the decreasing wind speed involves an increasing in the integration range of r. It follows that only a portion of the correlation function is contributing signi cantly to the scattering coef cient and this portion is controlled by the frequency and how fast the correlation function decays (as a function of wind speed). The in uence of these parameters is not restricted to the SSA model, it is present also in the *Kirchhoff formulation* and in the scattering model named *Integral Equation Model (IEM)* [4]. It is important to note that effective parameters are selected under a given system and geometric condition. Thus, they do not have general validity. For example, effective surface parameters selected to explain backscattering cannot be used to explain scattering along the specular direction (gure 2).

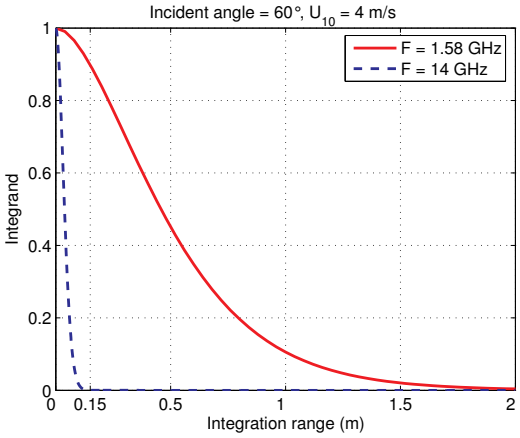

(a)

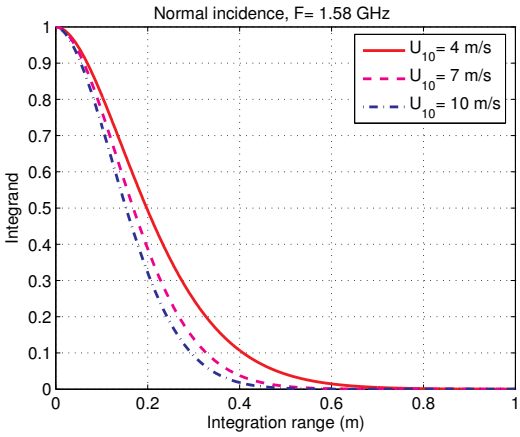

(b)

Fig. 2. Integrand evaluation in specular direction for a correlation function calculated from Elfouhaily's spectrum (a) Comparison between results obtained in L-band and K_u-band (b) Integrand dependence on wind speed for L-band

III. A SEA SURFACE CORRELATION FUNCTION

In this section we want to show that the surface has a correlation function quite different from a Gaussian or an exponential and that it is a very strong wind dependence. To illustrate these points, we use the Elfouhaily *et al* [13] sea spectral model which was developed solely from in situ or tank measurements, along with physical arguments. It is noteworthy that this model was developed without any relation to remote-sensing data.

Elfouhaily *et al* assume a directional spectrum $S(K,\psi)$ defined in polar coordinates as

$$S(K,\psi) = S(K)f(K,\psi) \tag{4}$$

where

$$S(K) = (B_L + B_H)/K^3 \tag{5}$$

and

$$f(K,\psi) = [1 + \Delta(K)\cos(2\psi)]/2\pi \tag{6}$$

In (4), $S(K)$ denotes the non-directional spectrum (isotropic part) modulated by the $f(K,\psi)$ spreading function. In (5), B_L and B_H are the respective contributions from low (gravity waves) and high (cappliray waves) wavenumbers. ψ is the azimuthal angle measured with respect to the mean wind direction. The factor $\cos(2\psi)$ (6) is responsible to return the spectrum symmetric compared to the wind direction axis. It must be noted that the spectral value in the upwind case $(\psi = 0°)$ equal to that in the downwind $(\psi = 180°)$, in reality it is not the case but this phenomena is non-surprising because in this model the ocean surface follows Gaussian statistics. We avoided some deficiencies to this spectrum cited in [14][15]. This spectrum will be used in the next section when we evaluate bistatic sea scattering cross section.

The surface correlation function is related to the spectrum by the following definition:

$$\rho(r,\phi) = \int_0^{\infty}\int_0^{2\pi} S(K,\psi) \times exp[iKr\cos(\psi-\phi)Kd\phi\ dK] \tag{7}$$

The sea height correlation function is then expressed in polar coordinates, $\boldsymbol{r} = (r_x, r_y) = (r\cos\phi, r\sin\phi)$

$$\rho(r,\phi) = \rho_0(r) - \cos(2\phi) \times \rho_2(r) \tag{8}$$

$$\begin{cases} \rho_0(r) = \int_0^{\infty} S(K)J_0(Kr)dK \\ \rho_2(r) = \int_0^{\infty} S(K)J_2(rK)\Delta(K)dK \end{cases} \tag{9}$$

$\rho_0(r)$ is the isotropic part, whereas $\rho_2(r)$ denotes the anisotropic part. J_n is the th-order Bessel function of the first kind. It must noted that which explains that the upwind/downwind asymmetry cannot be predicted.

Figure 3 shows the normalized correlation function based on Elfouhaly's spectrum for two wind speed U_{10}= 4 and 7 m/s (defined at 10 meters above the surface) along upwind, cross wind directions and for an angle equal to $45°$ with respect to the mean wind direction. The simulations were made for an inverse wave age of 0.84, corresponding to fully developed sea.

Note that the correlation length increases very quickly with the wind speed and that there is a significant range of negative values not present in most correlation functions for land surfaces. This is a clearly a narrow band process and hence the sea surface autocorrelation function is not at all describable by a Gaussian correlation function, as has sometimes been assumed in the past [16]. Another special property of the sea correlation function is that it integrates to zero, because $S(0,\psi)$ is zero. Thus, it makes a big difference how far we integrate and this dependent on the values of $\kappa \cdot \rho(0)$ and the rate of decay of the correlation function (see figure 2). If we examine the computed values of $\rho(0)$ for three wind

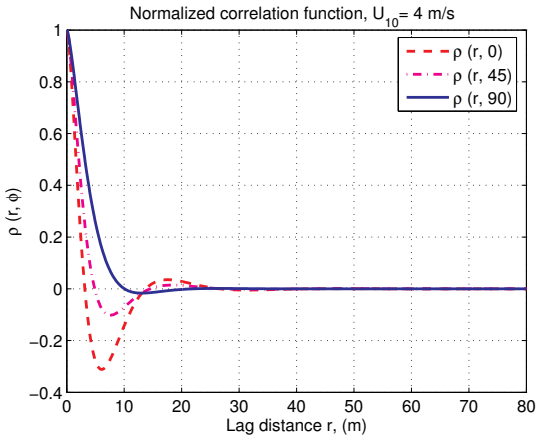

(a)

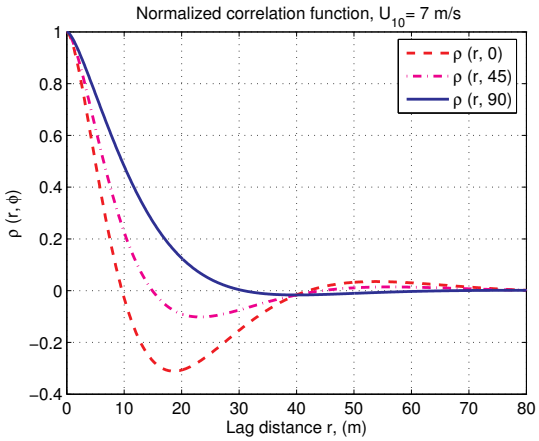

(b)

Fig. 3. Normalized correlation functions of the sea surface simulated with Elfouhaily sea spectrum. (a) $U_{10} = 4m/s$ and (b) $U_{10} = 4m/s$. $\rho(r, 0)$ and $\rho(r, 90)$ denote correlation function in upwind and cross wind directions, respectively

speed $\{4,\ 7,\ 10$ m/s$\}$ and κ at 1.58 GHz we can verify that except for the 4 m/s wind speed the negative portion of the correlation function is not encountered in integration over 0-80° incident angles for the specular direction cases (for a concrete illustration see figures 3 and 6). It is important to note that the evaluation of the 2-D correlation function $\rho(\boldsymbol{r})$ throughout the area of integration in (1) increases the computing time especially for large incidence angles.
The next section is dedicated to predict the NBCS of the sea surface by using the SSA scattering model seen in section II with a sea surface correlation function calculated from the Elfouhaily sea spectrum described in section III.

IV. Numerical results

This section is predicted to present numerical results of the NBCS of the 2-D anisotropic ocean surface at 1.58 GHZ (L-band) in several bistatic configurations : along the specular direction, in the forward scattering configuration, and in the fully bistatic one. Numerical results are obtained as a function of wind speed, incident/scattering angles and polarization states.

A. Scattering along the specular direction

In first time, we calculate the scattering coefficient behavior along the specular direction at 1.58 GHz from the sea surface as a function of wind speed velocity and incident angles. This is done by using the correlation function of the previous section in the SSA bistatic scattering model expressed in (1). It is important to note that the computed result for σ_{pp} along the specular direction is of major interest to bistatic sensing of the scattered signal from the GPS [4].
It must be noted that all simulations presented along the specular direction are made in upwind case. Figure 4 shows the SSA results along the specular direction at 1.58 GHz for three wind speed U_{10}=$\{4,\ 7,\ 10$ m/s$\}$. In examining graphs in figure 4, we can note a remarkable behavior at a wind speed of 4 m/s, that because the contribution of the negative region correlation function in the scattering computation at this wind velocity (as noted in the last section). At this velocity (4 m/s), the horizontally polarized coefficient is seen to rise with the incident angle until about 70° (figure 4). This rise is associated with both an increase in reflectivity and a decrease in κ resulting in a larger range over the positive portion of the sea surface correlation (figure 3). Beyond 70°, the scattering coefficient turns back down (figure 4). This down turn is due to integration into the negative correlation region. Nevertheless, at the two other wind speeds 7 and 10 m/s this behavior does not exist. Indeed , the surface rms height is much larger than that at 4 m/s. This yields a larger $\kappa\rho$ which restricts the range of integration to a smaller value than at 4 m/s and causes a decrease in the value of the NBCS (scattering coefficient). Physically, this decrease is due to an increase in the mean square slope associated with a higher wind speed. This narrowing of the range of integration has avoided the negative correlation region and hence the horizontally polarized scattering coefficient continues to rise with the incident angle up to 80°.

To underline this point clearly, we plot in figure 5 with the same parameters used in figure 4 for a waves frequency of 14 GHz. It is clear that at 4 m/s the down turn does not exist on the horizontally polarized coefficient as it is the case at 1.58 GHz frequency. This different behavior between results at 14 GHz and 1.58 GHz gives more credibility to the increase of the frequency in studying bistatic scattering problem from a sea rough surface especially near the grazing incident/scattering angles.

It must be noted that the major portion of the integrand in (3) is dependent on the function $\{e^{-\kappa[\rho(0)-\rho(r)]} - e^{-\kappa\rho(0)}\}$ where $\rho(0)$ is proportional to the mean square height and $\rho(\boldsymbol{r})$ is proportional to the mean square slope of the surface. The level of scattering is dependent on the combined effect of both height and slope. For a wind speed of 4 m/s, $\kappa \cdot \rho(0)$ is less than 50 at normal incidence and 1.58GHz. Mathematically, this value is not large enough to force the scattering integral to approach the high frequency limit. That means, in calculations

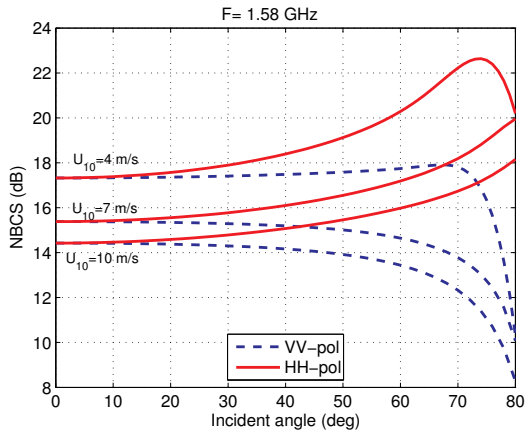

Fig. 4. Comparison between SSA results along the specular direction for vertical and horizontal polarization for three wind speed U_{10}={4, 7, 10 m/s}. The relative dielectric constant of water is taken to be 73-j58 at 1.58 GHz

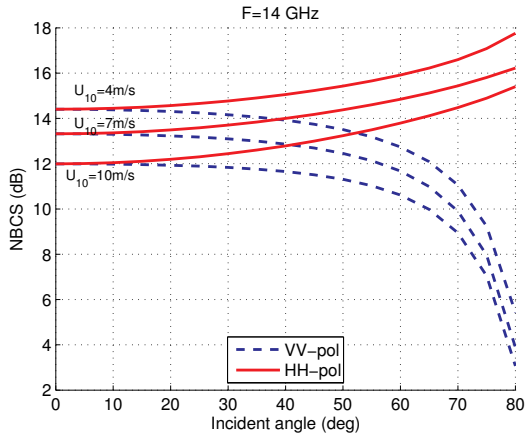

Fig. 5. Comparison between SSA results along the specular direction for vertical and horizontal polarization for three wind speed U_{10}={4, 7, 10m/s}. The relative dielectric constant of water is taken to be 47-j38 [17] at 14 GHz

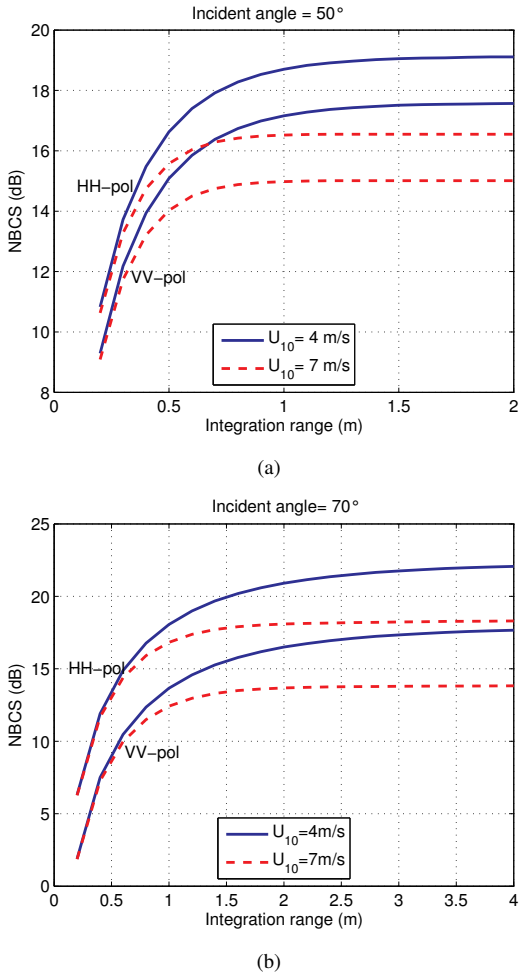

Fig. 6. Convergence of the scattering integral at 1.58 GHz for two wind speed 4 and 7 m/s as a function of the lag distance, (a) $\theta = 50°$ and (b) $\theta = 70°$

of the integral in (3) there is a significant range to be integrated over. This point is illustrated in figure 6 where it is shown that at 7 m/s convergence of the integral along the specular direction requires integration over the lag distance about 1 m where the incident angle equal to $50°$. For the same angle at wind speed of 4 m/s the integration range increases to about 2 m. Indeed, with increasing incident angle to $70°$ a large surface is needed to be integrated over, up to about 4 m at wind speed of 4m/s.

In figure 7 we have chosen to compare SSA results with the geometric optics of the Kirchhoff approximation (KA-GO) where this model is widely used for modeling the quasi-specular forward scattering. It must be noted that the KA-GO works well in the near-specular directions and gives inaccurate results in the direction far from specular, where the Bragg mechanism produces scattering of the same order of calculation [18].

In this comparison we fixed wind speed at 7 m/s and we plot NBCS along the specular direction in the range incidence $0 - 80°$. There is a good concordance between two results of the two models for incident angle until about $50°$. Beyond this value, the divergence between them appears and increases with increasing incident angle. At incident angle of $50°$ the amplitude obtained with SSA model is higher than for the KA-GO one by about 2 dB. This is because the SSA model at its first order take account relatively Bragg scattering. This result helps to determine the region of applicability of the KA-GO, therefore reveals some effects can not be obtained using the KA-GO.

B. Forward scattering

The objective of the results in this part is to examine the forward scattering configuration which is also one of major interest to bistatic sensing of the scattered signal from the GPS. We recall that the numerical computations are evaluated with the SSA scattering model.

Figure 8 shows the SSA results at 1.58 GHz in the forward scattering configuration. The incident angle is fixed to $30°$,

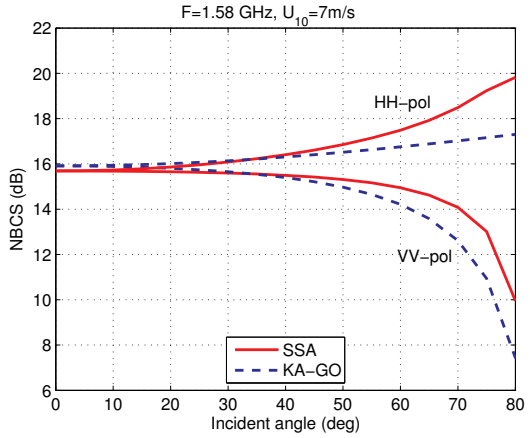

Fig. 7. Comparison between SSA and KA-GO results along the specular direction for vertical and horizontal polarization at a wind speed of 7 m/s

azimuthal angles are the same for incident and scattered radiation ($\varphi = \varphi_s$), and we vary the wind speed from 5 to 15m/s. In the part (a) of this figure, the VV-polarization case is dressed and in part (b) the HH-one.

As is apparent in figure 8 , the maximum energy is received around the specular direction $30°$ which is logical result (incident angle equal to $30°$). This maximum decreases when the wind speed increases.

In figure 9 we evaluate the NBCS in forward case for three incident angle $\theta = \{30°, 40°, 50°\}$ at wind speed of 5 m/s for VV- and HH-polarization. An important remark appears from figure 9 that the maximum of the energy obtained is quasi independent on the incident angle value. For small scattering angles the results of $30°$ is higher than of $40°$ and $50°$. while for large scattering angles the inverse behavior takes place.

In figure 10 we present an illustration of the KA-GO behavior in forward scattering configuration for an incident angle of $30°$ and at a wind speed of 5 m/s. In examining the graphs of this figure a good agreement between SSA and KA-GO results for scattering angles $\pm 25°$ around the specular direction. A departure takes place for wider scattering angles where a contribution from Bragg scattering cannot be neglected.

C. Scattering in fully bistatic configuration

A study on the fully bistatic configuration with the SSA model in K_u-band was made where a comparison with Two Scale Model was accomplished [10].

In figure 11 we present numerical simulations in fully bistatic configuration by changing the scattering azimuth direction. Incident and scattering angles are fixed to $40°$ and $60°$. By varying the azimuth angle from $0°$ to $180°$, we obtain several particular configurations. The zero corresponds to forward scattering and an azimuth value of $180°$ represents the backscattering case. For the direction orthogonal to incident plane, the azimuth angle equal to $90°$.

There is a translation of the peak for VV-pol with increasing incident/scattering angle, where in HH-one its placed is

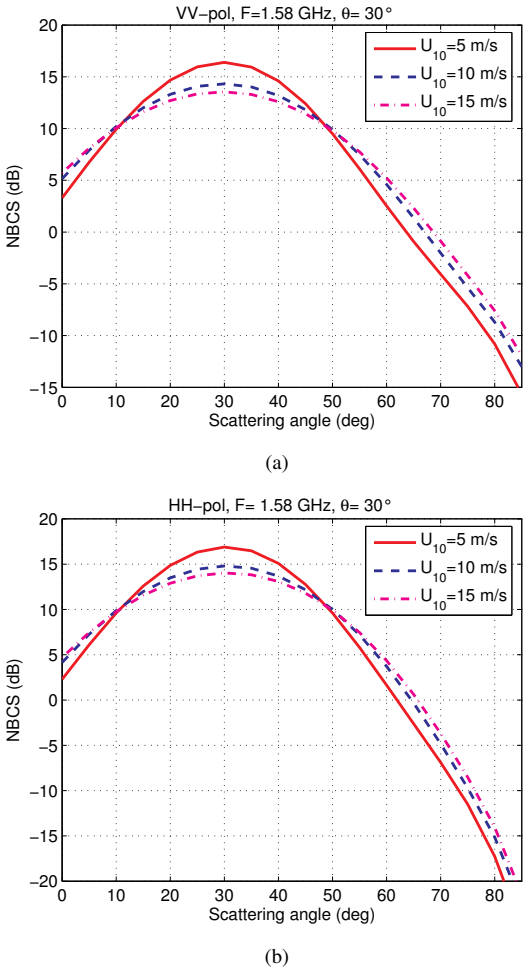

Fig. 8. NBCS results obtained with SSA model in forward scattering configuration as a function of scattering angle at 1.58 GHz and incident angle equal to $30°$ for three wind speed $U_{10} = \{5, 10, 15m/s\}$ in upwind direction (a) for VV-polarization and (b) HH-polarization

always in the direction orthogonal to incident plane (scattering azimuth=$90°$). The presence of the peak signifies a non physical phenomena which must be analyzed deeply.

With the same parameters as in figure 11 we plot in figure 12 the SSA results for cross-polarization cases. It must be noted that VH-pol scattering coefficient is equal to HV-one in case. We can note that for scattering angles strictly near the nadir zone ($0°$-$10°$) there is not an influence when the incident angle increase from $40°$ to$60°$. Yet, for moderate and large scattering angles the NBCS values decreases with increasing incident angles.

V. Conclusion

In this paper we have studied the scattering from the sea surface at L-band by combining the SSA scattering model and the Elfouhaily sea spectrum model. The correlation function based on this spectrum was calculated then the influence of the negative part of this function is discussed. At L-band, for small wind speed the computation of the NBCS need

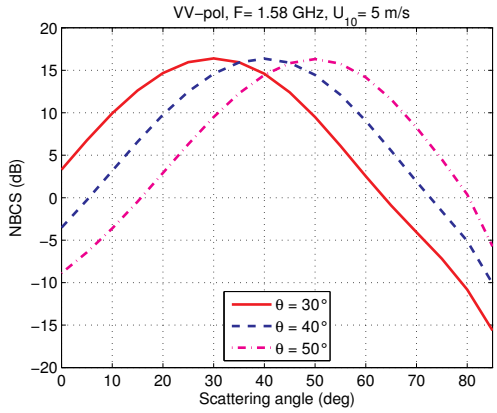

(a)

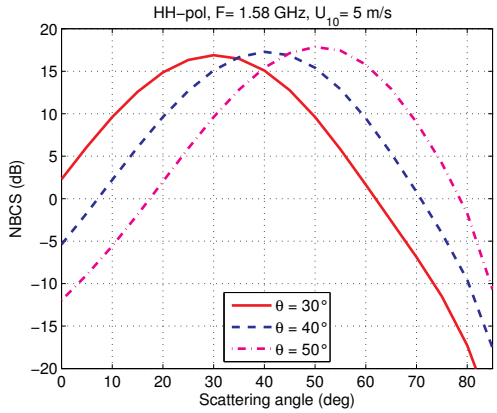

(b)

Fig. 9. NBCS results obtained with SSA model in forward scattering configuration as a function of scattering angle at 1.58 GHz at wind speed of $U_{10} = 5m/s$ for three incident angles $\{30°, 40°, 50°\}$ in upwind direction (a) for VV-polarization and (b) for HH-polarization

an integration over a negative portion of this function which cause a down turn in scattering along the specular direction for large incident angles. Nevertheless, it is not the case at K_u-band (F=14 GHz). A good concordance between the SSA model and KA-GO appears for incident angles less than $50°$ in the specular direction case, while a difference to about 1-2 dB for larger angles. This comparison helps to determine the region of applicability of the KA-GO. The fully bistatic case is also studied where a non physical phenomena appears by the peak presence. This work can be considered as an attempt to introduce SSA in the GPS when this system is used as a remote sensing tool.

REFERENCES

[1] J. Martin-Neira, C. Mavrocordatos, and E. Colzi, "Study of a constellation of bistatic radar altimetters for mesoscale ocean applications," *IEEE trans. Geosci. Remote Sensing*, vol. 36, pp. 1898–1904, 1998.

[2] V. U. Zavorotny and A. V. Voronovich, "Scattering of GPS signals from the ocean with wind remote sensing application," *IEEE trans. Geosci. Remote Sensing*, vol. 38, no. 2, pp. 951–964, 2000.

[3] T. Elfouhaily and B. Chapron, "A physically-based two-scale electromagnetic model for backscatter from ocean-like surfaces," *in Proc. IGARSS*, pp. 600–602, 1996.

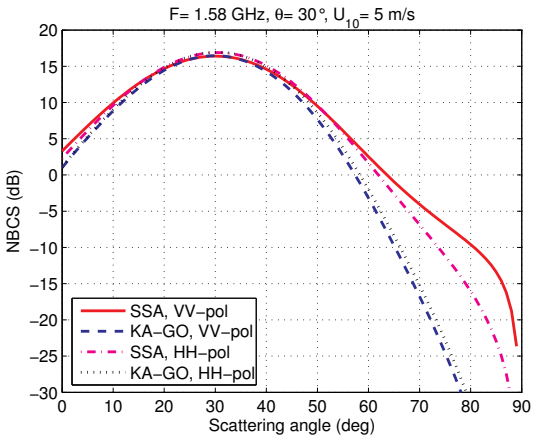

Fig. 10. Comparison between SSA and KA-GO results in forward scattering configuration for vertical and horizontal polarization at a wind speed of 5 m/s

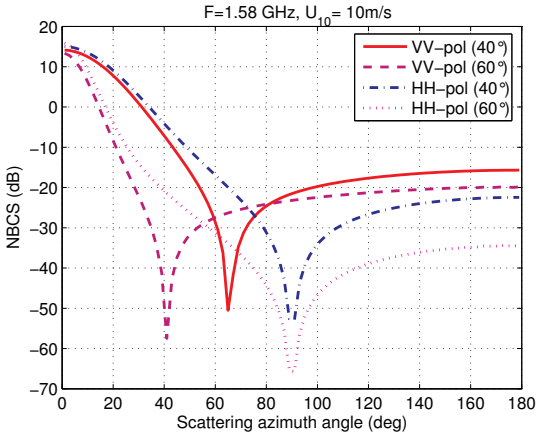

Fig. 11. NBCS variations for co-polarization cases in fully bistatic configuration as a function of scattering azimuth angle φ_s at 1.58 GHz and U_{10}= 10 m/s. Incident angle is fixed to $40°$ and $60°$

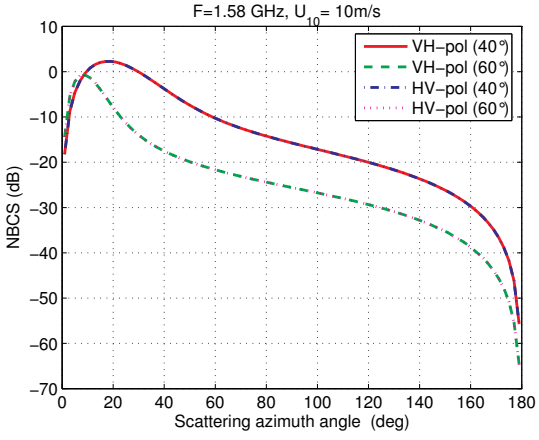

Fig. 12. NBCS variations for cross-polarization cases in fully bistatic configuration as a function of scattering azimuth angle φ_s at 1.58 GHz and U_{10}= 10 m/s. Incident angle is fixed to $40°$ and $60°$

[4] A. K. Fung, C. Zuffada, and C. Y. Hsieh, "Incoherent bistatic scattering from the sea surface at l-band," *IEEE trans. Geosci. Remote Sensing*, vol. 39, no. 5, pp. 1006–1012, 2001.
[5] A. Coatanhay and A. Khenchaf, "Model of GPS signal from the ocean based on an electromagnetic scattering theory: Two Scale Model (TSM) approach," *in Proc. IGARSS*, 2005.
[6] D. R. Thompson, T. M. Elfouhaily, and J. L. Garrison, "An improved geometrical optics model for bistatic GPS scattering from the ocean surface," 2005.
[7] T. Elfouhaily and C. A. Guérin, "A critical survey of approximate scattering wave theories from random rough surfaces," *Waves Random Media*, vol. 14, pp. R1–R40, 2004.
[8] A. G. Voronovich and V. U. Zavorotny, "Theoretical model for scattering of radar signals in k_u- and c-bands from a rough sea surface with breaking waves," *Waves Random Media*, vol. 11, pp. 247–269, 2001.
[9] A. Khenchaf, "Bistatic scattering and depolarization by randomly rough surfaces: application to the natural rough surfaces in X-band," *Waves Random Media*, vol. 11, pp. 61–89, 2001.
[10] A. Awada, A. Khenchaf, A. Coatanhay, and M. Y. Ayari, "Comparison between small slope approximation and two scale model in bistatic configuration," *in The proceedings of the IEEE International Geoscience and Remote Sensing Symposium*, pp. 1341–1344, Seoul, Korea 2005.
[11] A. G. Voronovich, "Small-slope approximation for electromagnetic wave scattering at a rough interface of two dielectric half-spaces," *Waves Random Media*, vol. 4, pp. 337–367, 1994.
[12] M. Abramowitz, *Handbook of mathematical functions*, 9th ed. Dover Publications, 1972.
[13] T. Elfouhaily, B. Chapron, K. Katsaros, and D. Vandemark, "A unified directional spectrum for long and short wind-driven waves," *J. Geophys. Res.*, vol. 102, no. C7, pp. 781–796, 1997.
[14] A. Lemaire, P. Sobieski, and A. Guissard, "Full-range sea surface spectrum in nonfully developed state for scattering calculations," *IEEE trans. Geosci. Remote Sensing*, vol. 37, pp. 1038–1051, 1999.
[15] S. T. McDaniel, "Small-slope predictions of microwave backscatter from the sea surface," *Waves Random Media*, vol. 11, pp. 343–360, 2001.
[16] J. R. Apel, "An improved model of the ocean surface wave vector spectrum and its effects on radar backscatter," *Journal. Geo. Res.*, vol. 99, no. C7, pp. 16,269–16,291, 1994.
[17] A. Ellison, A. Balana, G. Delbos, K. Lamkaouchi, L. Eymard, C. Guillou, and C. Prigent, "New permittivity measurements of seawater," *Radio. Sci.*, vol. 33, pp. 639–648, 1998.
[18] V. U. Zavorotny and A. V. Voronovich, "Bistatic radar scattering from an ocean surface in the small-slope approximation," *in Proc. IGARSS*, pp. 2419–2421, 1999.